JOURNAL OF VIROLOGY, June 2004, p. 6682–6687 Vol. 78, No. 12
0022-538X/04/$08.00+0 DOI: 10.1128/JVI.78.12.6682–6687.2004

NOTES

Target Specificity of Human Immunodeficiency Virus Type 1 NCp7 Requires an Intact Conformation of Its CCHC N-Terminal Zinc Finger

S. Ramboarina,* S. Druillennec, N. Morellet, S. Bouaziz, and B. P. Roques

Département de Pharmacologie Chimique & Génétique, INSERM U266, CNRS FRE 2463, UFR des Sciences Pharmaceutiques et Biologiques, 75270 Paris Cedex 06, France

Received 9 October 2003/Accepted 30 January 2004

The modification of zinc-binding residues inside the conserved CCHC motif of human immunodeficiency virus type 1 NCp7, in particular into CCHH, induces a complete loss of infectivity. Since the mutant His28NCp7 has been shown to be devoid of infectivity in vivo, the structure-function relationships of the mutant His28(12-53)NCp7 were investigated by nuclear magnetic resonance and surface plasmonic resonance. Although the Cys28→His mutation modifies drastically the structure of the core domain (residues 12 to 53) of NCp7, His28(12-53)NCp7 still interacts with a 10-fold-lower affinity to specific nucleic acid targets, such as SL3, a stem-loop critically involved in viral RNA packaging, and without affinity change with the nonspecific, single-stranded nucleic acid poly(T). Moreover, His28(12-53)NCp7 and native (12-53)NCp7 displayed the same affinity with reverse transcriptase, but the natures of the complexes are probably different, accounting for the drastic reduction in the amount of RNA packaged in the mutated virus. We propose a structural model of His28(12-53)NCp7 that provides insights into the NCp7 structural features necessary for target recognition and that shows that the specific native structure of the zinc finger domain is strictly required for the optimal target selectivity of NCp7.

Human immunodeficiency virus type 1 (HIV-1) NCp7 is a small basic protein that is well characterized as a nucleic acid chaperone protein involved in annealing and hybridization activities. NCp7 plays a crucial role in key steps of the viral life (6, 29). NCp7 contains two well-conserved $CX_2CX_4HX_4C$ zinc finger (ZF) motifs (Fig. 1) that are required for most of these processes (5, 9–13, 17, 18, 26, 30, 32–34). Nuclear magnetic resonance (NMR) of the structure of NCp7 of HIV-1 revealed that the two well-folded CCHC ZFs (21, 25, 31) are in close spatial proximity (16, 17, 20, 21, 22, 28). Strong relationships have been established between the three-dimensional organization of NCp7 and its biological functions. Mutations of the CCHC motif into CCCC or CCHH in the N-terminal ZF of NCp7 lead to a complete loss of infectivity (5, 8, 10, 12, 32, 34). In the case of CCCC, this behavior has been correlated with a loss of spatial proximity between the two ZFs (8), impeding nucleic acid interactions (17, 23), reverse transcriptase (RT) recognition (9), and optimal nucleic acid chaperone activities (13, 17, 34). Previously, it was shown that in the isolated N-terminal ZF, the Cys28→His mutation resulted in the formation of two folded interconverting forms, E and D, due to the coordination of zinc by His28 via $N^{\varepsilon 2}$ and its $N^{\delta 1}$ imidazole atoms, respectively (27). It has been shown that His28NCp7 was able to package only 32% of the viral RNA packaged by the wild type and that a defect in the reverse transcription process leads to a 10^4-fold decrease in infectivity (10).

In an effort to dissect the impact on NCp7 activity of the substitution of the CCHC motif for CCHH and CCCC in the N-terminal ZF of NCp7, we have used surface plasmonic resonance (SPR) to investigate the interactions of His28(12-53)NCp7 and Cys23(12-53)NCp7 (Fig. 1) with the specific relevant targets of NCp7, RT, and SL3 (a stem-loop of the viral RNA packaging domain) and with a nonspecific DNA sequence, poly(T). Although both mutations affect drastically the structure of the N-terminal ZF of NCp7 and induce mutated forms that are defective in vivo (10), they display radically different in vitro responses. In order to explain these differences at the molecular level, structural models of His28(12-53)NCp7 are proposed and compared to those of (12-53)NCp7 and Cys23(12-53)NCp7.

Ability of His28(12-53)NCp7 to interact in vitro with specific targets contrasted with that of Cys23(12-53)NCp7. The contribution of the N-terminal ZF in (12-53)NCp7 and its derivatives His28(12-53)NCp7 and Cys23(12-53)NCp7 in efficient nucleic acid binding or RT recognition was measured using SPR experiments by direct interaction with SL3 and RT. Figure 2A represents an overlay of the sensorgrams obtained from successive injections of each peptide solution. Dilute concentrations (200 nM) of peptides were used on immobilized 5′-biotinylated SL3 in HBS buffer (10 mM HEPES, 100 mM NaCl, 0.005% p20; pH 7.4) in order to avoid aggregation or oligomerization. Increasing concentrations of each peptide were injected at 30 μl/min for 100 s, and the dissociation was

* Corresponding author. Present address: Department of Biological Sciences, Imperial College of Sciences, Technology and Medicine, South Kensington Campus, London SW7 2AZ, United Kingdom. Phone: 44 207-594-5464. Fax: 44 207-594-5207. E-mail: s.ramboarina@imperial.ac.uk.

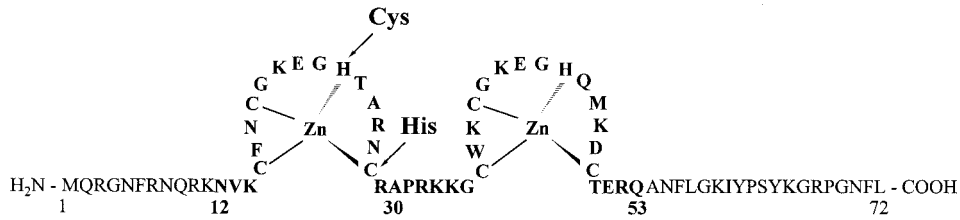

FIG. 1. Primary sequence of NCp7. The His23→Cys and Cys28→His mutations leading to CCCC and CCHH mutants are indicated by arrows. The domain from residues 12 to 53 of NCp7, which is critical for the biological activities of the protein, is indicated in bold.

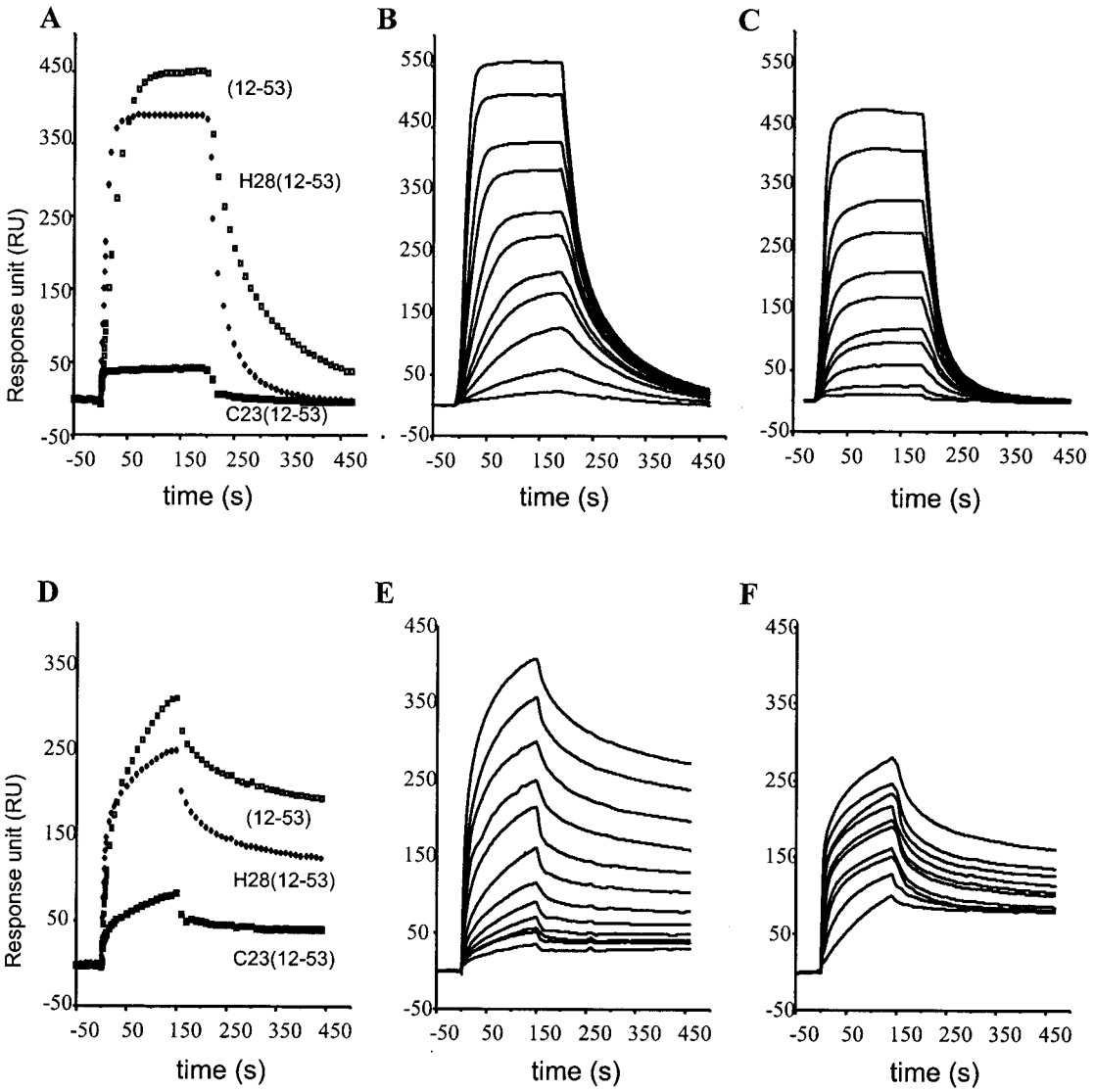

FIG. 2. Interaction of (12-53)NCp7 and its mutants Cys23(12-53)NCp7 and His28(12-53)NCp7 with the specific targets SL3 and RT. (A) Direct binding of (12-53)NCp7 and its mutants to SL3 as measured by the SPR method. The same concentration (200 nM) of (12-53)NCp7 [(12-53); ◆], His28(12-53)NCp7 [H28(12-53); ●], or Cys23(12-53)NCp7 [C23(12-53); □] was injected into 600 response units of SL3 immobilized on the sensor chip in HBS buffer at 25°C. (B and C) Kinetic analyses of the (12-53)NCp7/SL3 (B) and His28(12-53)NCp7/SL3 (C) complexes. Protein concentrations were allowed to vary from 500 to 7 nM (500, 375, 250, 187, 125, 93, 62, 46, 31, 15, and 7 nM). (D) Direct binding of (12-53)NCp7 and its mutants to RT. The same concentration (1.6 μM) of (12-53)NCp7 [(12-53); ■], His28(12-53)NCp7 [H28(12-53); ●], or Cys23(12-53)NCp7 [C23(12-53); □] was injected into 4,000 response units of RT immobilized on the sensor chip in HBS buffer at 25°C. (E and F) Kinetic analyses of (12-53)NCp7/RT (E) and His28(12-53)NCp7/RT (F) complexes. Protein concentrations were allowed to vary from 4 μM to 62.5 nM (4, 3, 2, 1, 1.5, 0.75, 0.5, 0.375, 0.250, 0.187, 0.125, and 0.625 μM).

TABLE 1. Kinetic parameters of the complexes formed by (12–53)NCp7, His28(12–53) NCp7, NCp7, and (a-D)NCp7 with SL3, poly(T), and RT

Protein complex	k_a (M^{-1} s^{-1})	k_d (s^{-1})	K_D[a]
(12–53)NCp7/SL3	2.50 ± 0.08 (10^5)	2 ± 0.2 (10^{-3})	9 nM
(12–53)NCp7/poly(T)	1.37 ± 0.12 (10^5)	38 ± 3.0 (10^{-3})	277 nM
(12–53)NCp7/RT	0.22 ± 0.03 (10^5)	37 ± 4.0 (10^{-3})	1,700 nM
His28 (12–53)NCp7/SL3	4.70 ± 0.30 (10^5)	46 ± 5.0 (10^{-3})	97 nM
His28 (12–53)NCp7/poly(T)	0.21 ± 0.03 (10^5)	5 ± 0.7 (10^{-3})	238 nM
His28 (12–53)NCp7/RT	1.06 ± 0.09 (10^5)	41 ± 7.0 (10^{-3})	400 nM
NCp7/SL3	8.03 ± 0.07 (10^4)	2.31 ± 0.11 (10^{-4})	2.87 nM
NCp7/poly(T)	3.25 ± 0.13 (10^4)	4.46 ± 0.05 (10^{-4})	13.7 nM
NCp7/RT	—	—	—
(a-D)NCp7/SL3	9.47 ± 0.17 (10^4)	7.76 ± 0.14 (10^{-3})	81.9 nM
(a-D)NCp7/poly(T)	2.79 ± 0.16 (10^4)	2.00 ± 0.09 (10^{-3})	71.7 nM
(a-D)NCp7/RT	—	—	—

[a] K_D, affinity constant; —, no SPR experiments were performed for the interactions of NCp7 and (a-D)NCp7 with RT (see the text and reference 9).

observed for 300 s (Fig. 2B and C). Analysis with the BIAevaluation software showed that the data fitted well to the pseudo first-order model appropriate for dilute concentrations. His28(12-53)NCp7 retains its ability to recognize SL3, whereas Cys23(12-53)NCp7 does not interact with SL3 (Fig. 2A). The same conclusions were obtained with a biotinylated 30-mer nonspecific sequence, poly(T) (data not shown). Accordingly, the structural changes induced by the His23→Cys mutation strongly modified the interaction of the ZF domain with d(ACGCC) (8, 23) or with *trans* activator response (TAR) RNA (17). Moreover, in vitro, this CCCC mutant was shown to be unable to initiate the annealing of $tRNA^{Lys,3}$ to the primer binding site, in contrast to its native counterpart (30).

His28(12-53)NCp7 presents an association rate constant (k_a) of 4.7×10^5 M^{-1} s^{-1}, which is not significantly different from that of the native peptide (2.5×10^5 M^{-1} s^{-1}) (Table 1). However, the higher dissociation constant (k_d) of the mutant demonstrates that the complex of His28(12-53)NCp7 and SL3 is less stable than that of (12-53)NCp7 and SL3. This is illustrated by the total dissociation of the mutant from SL3, while a part of the native peptide still remains bound to SL3 (Fig. 2B and C). The affinities of (12-53)NCp7 and His28(12-53)NCp7 for SL3 were estimated from the kinetic data to be 9 and 97 nM, respectively (Table 1). Kinetic constants have also been calculated for the 30-mer poly(T) (Table 1). Although the k_a and k_d values for (12-53)NCp7 are different from those found for His28(12-53)NCp7, the two proteins have similar global affinities for poly(T) of 0.277 and 0.238 μM, respectively. Therefore, it appears that His28(12-53)NCp7 is able to interact with nonspecific polynucleotides as tightly as the wild-type peptide does, but it is not as efficient at discriminating a specific sequence like SL3, suggesting that a conserved structure of the ZF domain is required for specific recognition of the packaging signal.

In contrast to Cys23(12-53)NCp7, His28(12-53)NCp7 is still able to form a complex with RT (Fig. 2D). Measurement of the apparent kinetic rates of His28(12-53)NCp7/RT binding (Fig. 2E and F) shows that the complex is characterized by a k_d value close to that of the (12-53)NCp7/RT complex (0.041 and 0.037 s^{-1}, respectively). However, the k_a value of the mutant is higher than that of the native peptide. The affinities of (12-53)NCp7 and His28(12-53)NCp7 for RT are 1.7 and 0.4 μM, respectively (Table 1).

It appears that His28(12-53)NCp7 is still capable of interacting with unstructured DNA with an affinity similar to that of (12-53)NCp7 but that it has a weaker affinity with SL3. Although an interaction still occurs between His28(12-53)NCp7 and RT, His28(12-53)NCp7 forms a complex with RT that is kinetically or thermodynamically different from that formed with the wild-type peptide. NCp7 interacts with the two substrates p66 and p51 of RT by means of its two ZFs, with the N-terminal ZF reinforcing the required structure of the catalytic HIV-1 RNase H domain, thus improving its activity. The structural changes observed in the mutated proximal ZF may alter this functional activity of NCp7. These results are in good agreement with the data obtained by Gorelick et al. with His28NCp7 (10), which indicated that the 10^4-fold decrease in infectivity observed for His28NCp7 is not directly related to the 70% reduction in RNA packaging, but rather to a defect in the reverse transcription.

We also analyzed the role of the flanking regions, as it has been shown that the N-terminal region (1–11) is involved in the interaction with SL3 (7). We measured the binding constants for NCp7/SL3, NCp7/poly(T), (a-D)NCp7/SL3, where (a-D)NCp7 corresponds to NCp7 with the two ZFs replaced with two Gly-Gly linkers (9), and (a-D)NCp7/poly(T) by SPR (Table 1), using experimental conditions similar to those described for (12-53)NCp7 peptides. A comparison of the affinities estimated for NCp7 and those obtained for (12-53)NCp7 (Table 1) shows that the presence of the flanking regions stabilizes NCp7/SL3 by only a factor of 3 but that it increases the affinity by a factor of 20 for poly(T). The affinities obtained for (a-D)NCp7/SL3 and (a-D)NCp7/poly(T) (Table 1) indicate that the two CCHC ZFs are important for the optimal selectivity of NCp7 for nucleic acid sequences. In addition, it has been demonstrated that the presence of the two ZFs of NCp7 is crucial for RT recognition since (a-D)NCp7 does not interact with RT (9). The contribution of the extremities of NCp7 seems to be low since the affinities of NCp7/RT and (12-53)NCp7/RT are 0.6 (9) and 1.7 μM, respectively.

NMR analysis of His28(12-53)NCp7. Since the Cys28→His mutation in the isolated N-terminal ZF modifies drastically the structure of the core domain (27), a structural study by NMR of His28(12-53)NCp7 was attempted in order to establish a correlation with the in vitro observations. This structure-function relationship of His28(12-53)NCp7 provides insights into the NCp7 structural features important for its functions during the retrovirus life cycle. We examined the effect of the Cys28→His mutation on the ZF domain of NCp7 using standard ^{1}H NMR methods as described previously (8, 21, 22, 27). A ^{1}H-^{15}N heteronuclear single-quantum correlation (HSQC) experiment (2) carried out from 278,000 (278K) to 293K on His28(12-53)NCp7 synthesized with a 95% ^{15}N-labeled His28 residue (27) shows that both the D and E conformations are still observed in the ZF domain of NCp7 (Fig. 3A). In the two-dimensional nuclear Overhauser effect spectroscopy (NOESY) (14, 19), we observed sharp peaks for the region encompassing residues 33 to 53 and containing the C-terminal ZF (data not shown), indicating that the latter is not affected by the interconversion of the CCHH ZF. The remainder are either broad or missing, indicating that the N-terminal CCHH ZF and a part of the linker are in slow or intermediate exchange on the NMR timescale. The first part of the linker is affected by the exchange in the CCHH ZF. We can assume that the D and E forms determined in the isolated CCHH ZF are still conserved in the domain from residues 12 to 53 since (i) NOESY performed at 278K in D_2O on His28(12-53)NCp7 showed similar NOE patterns and chemical shifts for the aromatic protons of Phe16, His23, and His28 (Fig. 3A) and (ii) the ^{15}N and ^{1}H chemical shifts of His28 in both forms are identical to those observed in the isolated CCHH ZF (Fig. 3B). Analysis of the peak intensities in the HSQC (Fig. 3B) indicates that the D form is a major conformation in His28(12-53)NCp7 but that the D and E forms were equally present in the isolated CCHH ZF (27).

These results indicate that the Cys28→His mutation induces different effects on the folding and dynamic behavior of the ZF domain to the His23→Cys mutation (8). The interactions between the linker and the N-terminal ZF probably favor the CCHH D form and suggest that cooperative behavior and transient interactions may occur between the N-terminal CCHH ZF and the linker in His28(12-53)NCp7, inducing some restricted motions in the linker.

Comparison of the models of His28(12-53)NCp7 with the wild-type (12-53)NCp7 structure. We attempted to generate three-dimensional models of His28(12-53)NCp7 using standard procedures in X-PLOR version 3.84 (4, 24). The distance restraints observed in the isolated CCHH ZF (27) were used for His28(12-53)NCp7. Those identified by NOESY for residues 34 to 53 were identical to those in the native (12-53)NCp7 (21, 22) and were introduced into the calculations. Ten structures over 100 were retained for each form based on the lowest total energy; no NOE violations were greater than 0.2 Å, and no angle violations were greater than 5°. The quality of the structures was evaluated with PROCHECK (15).

Due to the absence of restraints between the two ZFs in the calculations, no model shows proximity between the CCHH and CCHC ZFs (Fig. 4). In contrast to the isolated CCHH ZF, where the average root mean square distance (RMSD) on the Cys15-His28 backbone atoms was less than 0.5 Å for both

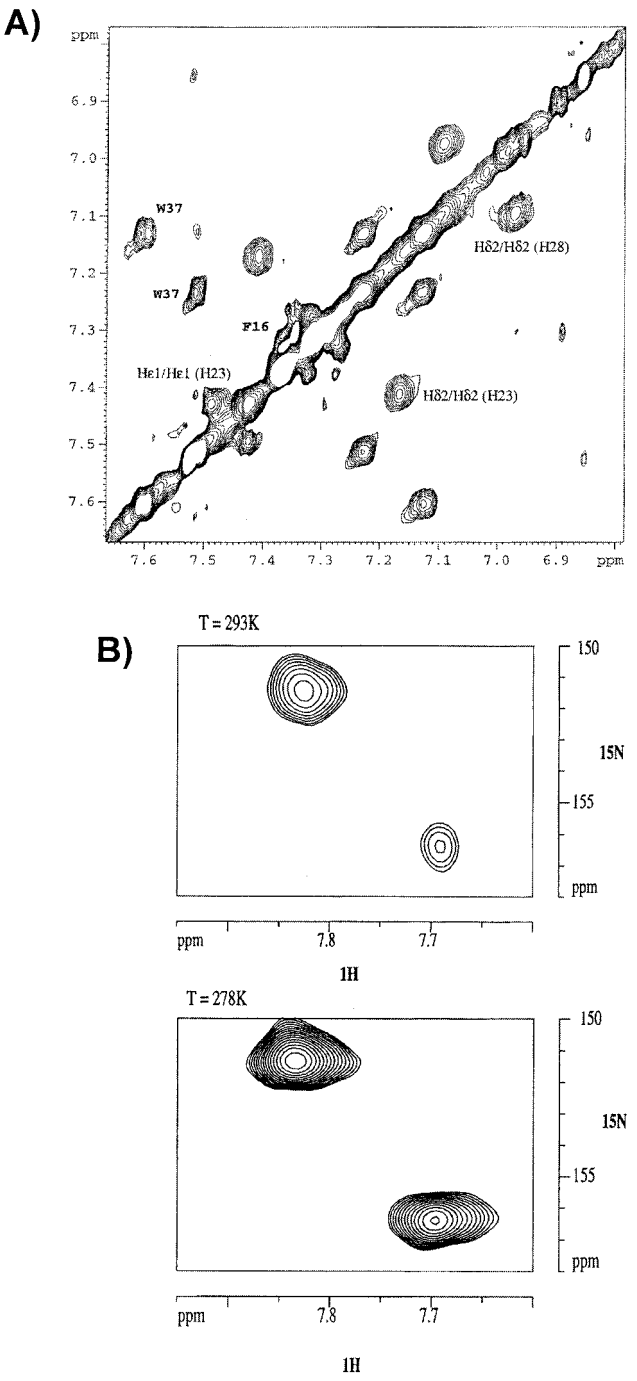

FIG. 3. Evidence of two forms in exchange in His28(12-53)NCp7. (A) Fingerprint aromatic region of the NOESY spectrum of His28(12-53)NCp7 in D_2O at 278K showing chemical exchange cross-peaks for the His23 ring protons $H^{\delta 2}$ and $H^{\varepsilon 1}$ and for His28 $H^{\delta 2}$. The aromatic protons of Trp37 in the second ZF remained unaffected by the chemical exchange occurring at the N-terminal CCHH ZF level. (B) ^{1}H-^{15}N HSQC analysis at 293K (top) and at 278K (bottom) of His28(12-53)NCp7 in which only His28 is ^{15}N enriched. Two ^{1}H-^{15}N correlation peaks evidenced at 7.82 and 7.68 ppm in the ^{1}H dimension for His28 show the presence of both the D and E forms, respectively. A smaller relative intensity of peaks is observed at 278K than at 293K, indicating the stabilization of the E form with a decrease of temperature.

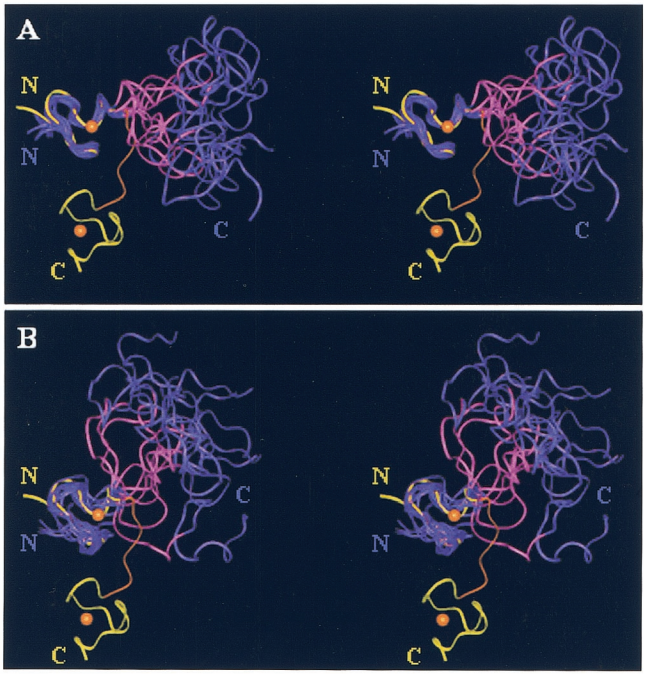

FIG. 4. Comparison of the D and E forms of His28(12-53)NCp7 with those of (12-53)NCp7. (A and B) Stereoviews showing the superimposition of the 10 lowest-energy structures of the D form (A) and E form (B) of His28(12-53)NCp7 on the native (12-53)NCp7 structure. In both the D and E forms of His28(12-53)NCp7 (in purple, with the linker in magenta), the N-terminal residues from positions 15 to 28 of the CCHH ZF are superimposed on the native N-terminal residues of the CCHC ZF of (12-53)NCp7 (in yellow, with the linker in orange). The average RMSD values on the Cys15-His28 backbone atoms on the 10 models of both the D and E forms in His28(12-53)NCp7 are 1.10 ± 0.21 and 2.26 ± 0.21 Å, respectively.

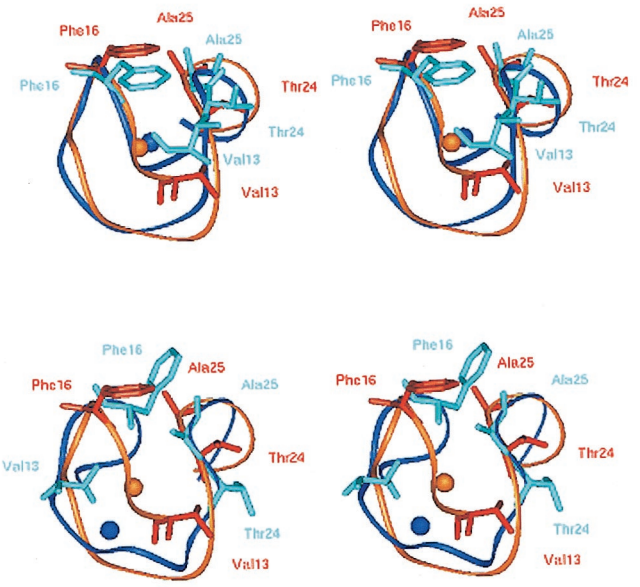

FIG. 5. Comparison of the side chain orientations of the mutant CCHH and the native CCHC structures. Stereoview of the N-terminal CCHH ZF of the best model of both the D (top) and E (bottom) forms (dark blue) superimposed on the N-terminal CCHC ZF of the native (12-53)NCp7 (orange). The RMSD values for the Cys15-His28 backbone atoms between the N-terminal native CCHC ZF and those of the best models of both the CCHH D and E forms are 1.49 and 2.28 Å, respectively. Side chains of Val13, Phe16, Thr24, and Ala25 are shown in light blue for the D and E forms of His28(12-53)NCp7 and in red for the native (12-53)NCp7. These four residues, essential for the interaction with nucleic acids, form a cluster in the D form that is similar to that observed in the native (12-53)NCp7.

forms (27), the average backbone RMSD values on the 10 lowest-energy models of both D and E CCHH forms in His28(12-53)NCp7 are 1.10 ± 0.21 and 2.26 ± 0.45 Å, respectively (Fig. 4). These calculations give an indication of how the linker and the C-terminal ZF can act on the relative distributions of both D and E forms. This is consistent with the NMR results that show that D is the most stable form of His28(12-53)NCp7.

Comparison of the models of lowest energy for both forms with the native ZF indicates that the CCHH D form of His28(12-53)NCp7 is closer to the native CCHC fold, with an average backbone RMSD of 1.49 Å compared to 2.28 Å for the E form (Fig. 5). In addition, it appears that, in contrast to the E form, the side chains of residues involved in the nucleic acid interactions (Val13, Phe16, Thr24, and Ala25) (1, 2, 7, 23) form a cluster in the D form similar to that observed in the first CCHC ZF in the wild-type NCp7 (Fig. 5). Conversely, this cluster is not observed in the Cys23(12-53)NCp7 structure (8). Recent studies have shown that the first and second ZFs in NCp7 are not interchangeable for the NCp7 nucleic acid chaperone activity (13, 17) and suggested that the optimal unwinding activity could be attributed to the hydrophobic cluster in the first ZF of NCp7 that is not present in the second ZF (17). Based on our structural models of His28(12-53)NCp7 and Cys23(12-53)NCp7 and their different in vitro responses observed by SPR, it appears that the formation of the hydrophobic cluster in the first ZF may be a critical factor for nucleic acid interaction and RT recognition.

Conclusion. In spite of the conformational heterogeneity of the His28(12-53)NCp7 mutant, our study suggests that some His28(12-53)NCp7 conformations may be closer to that of the native (12-53)NCp7 than to those of Cys23(12-53)NCp7. This may account for the interaction of His28(12-53)NCp7 with NCp7 targets observed by SPR. However, our results indicate that the integral structure of the first ZF of NCp7 is required for viral DNA synthesis via an optimal interaction between NCp7 and RT for maintaining HIV infectivity.

The structures of His28(12-53)NCp7 were deposited in the Protein Data Bank with the code numbers 1Q3Y and 1Q3Z for the D and E forms of His28(12-53)NCp7, respectively.

We thank Patrice Petitjean for ^{15}N-His28(12-57)NCp7 peptide synthesis.

This work was supported by grants from the Agence Nationale de la Recherche sur le SIDA (ANRS), SIDACTION, and the Ministère de l'Enseignement Supérieur et de la Recherche (MESR). S.R. was supported by a grant from MESR.

REFERENCES

1. **Amarasinghe, G. K., R. N. De Guzman, R. B. Turner, K. J. Chancellor, Z. R. Wu, and M. F. Summers.** 2000. NMR structure of the HIV-1 nucleocapsid protein bound to stem-loop SL2 of the Ψ-RNA packaging signal. Implications for genome recognition. J. Mol. Biol. **301:**491–511.
2. **Amarasinghe, G. K., J. Zhou, M. Miskimon, K. J. Chancellor, J. A. Mc-**

Donald, A. G. Matthews, R. R. Miller, M. D. Rouse, and M. F. Summers. 2001. Stem-loop SL4 of the HIV-1 Ψ RNA packaging signal exhibits weak affinity for the nucleocapsid protein. Structural studies and implications for genome recognition. J. Mol. Biol. **314:**961–970.

3. **Bodenhausen, G., and D. J. Ruben.** 1980. Natural abundance nitrogen-15 NMR by enhanced heteronuclear spectroscopy. Chem. Phys. Lett. **69:**185–188.
4. **Brünger, A. T.** 1992. X-PLOR: software manual, version 3.1. Yale University Press, New Haven, Conn.
5. **Buckman, J. S., W. J. Bosche, and R. J. Gorelick.** 2003. Human immunodeficiency virus type 1 nucleocapsid Zn^{2+} fingers are required for efficient reverse transcription, initial integration processes, and protection of newly synthesized viral DNA. J. Virol. **77:**1469–1480.
6. **Darlix, J. L., M. Lapadat-Tapolsky, H. de Rocquigny, and B. P. Roques.** 1995. First glimpses at structure-function relationships of the nucleocapsid protein of retroviruses. J. Mol. Biol. **254:**523–537.
7. **De Guzman, R. N., Z. R. Wu, C. C. Stalling, L. Pappalardo, P. N. Borer, and M. F. Summers.** 1998. Structure of the HIV-1 nucleocapsid protein bound to the SL3 psi-RNA recognition element. Science **279:**384–388.
8. **Déméné, H., C. Z. Dong, M. Ottmann, M. C. Rouyez, N. Jullian, N. Morellet, Y. Mély, J. L. Darlix, M. C. Fournié-Zaluski, S. Saragosti, and B. P. Roques.** 1994. 1H NMR structure and biological studies of the His23→Cys mutant nucleocapsid protein of HIV-1 indicate that the conformation of the first zinc finger is critical for virus infectivity. Biochemistry **33:**11707–11716.
9. **Druillennec, S., A. Caneparo, H. De Rocquigny, and B. P. Roques.** 1999. Evidence of interactions between the nucleocapsid protein NCp7 and the reverse transcriptase of HIV-1. J. Biol. Chem. **274:**11283–11288.
10. **Gorelick, R. J., T. D. Gagliardi, W. J. Bosche, T. A. Wiltrout, L. V. Coren, D. J. Chabot, J. D. Lifson, L. E. Henderson, and L. A. Arthur.** 1999. Strict conservation of the retroviral nucleocapsid protein zinc finger is strongly influenced by its role in viral infection processes: characterization of HIV-1 particles containing mutant nucleocapsid zinc-coordinating sequences. Virology **256:**92–104.
11. **Guo, J., T. Wu, J. Anderson, B. F. Kane, D. G. Johnson, R. J. Gorelick, L. E. Henderson, and J. G. Levin.** 2000. Zinc finger structures in the human immunodeficiency virus type 1 nucleocapsid protein facilitate efficient minus- and plus-strand transfer. J. Virol. **74:**8980–8988.
12. **Guo, J., T. Wu, B. F. Kane, D. G. Johnson, L. E. Henderson, R. J. Gorelick, and J. G. Levin.** 2002. Subtle alterations of the native zinc finger structures have dramatic effects on the nucleic acid chaperone activity of human immunodeficiency virus type 1 nucleocapsid protein. J. Virol. **76:**4370–4378.
13. **Heath, M. J., S. S. Derebail, R. J. Gorelick, and J. J. DeStefano.** 2003. Differing roles of the N- and C-terminal zinc fingers in human immunodeficiency virus nucleocapsid protein-enhanced nucleic acid annealing. J. Biol. Chem. **278:**30755–30763.
14. **Jeener, J., B. H. Meier, P. Bachman, and R. R. Ernst.** 1979. Investigation of exchange processes by two-dimensional NMR spectroscopy. J. Chem. Phys. **71:**4546–4553.
15. **Laskowski, R. A., J. A. C. Rullman, M. W. MacArthur, R. Kaptein, and J. M. Thornton.** 1996. AQUA and PROCHECK-NMR: programs for checking the quality of protein structures solved by NMR. J. Biomol. NMR **8:**477–486.
16. **Lee, B. M., R. N. De Guzman, B. G. Turner, N. Tjandra, and M. F. Summers.** 1998. Dynamical behavior of the HIV-1 nucleocapsid protein. J. Mol. Biol. **279:**633–649.
17. **Lee, N., R. J. Gorelick, and K. Musier-Forsyth.** 2003. Zinc finger-dependent HIV-1 nucleocapsid protein-TAR RNA interactions. Nucleic Acids Res. **31:**4847–4855.
18. **Lener, D., V. Tanchou, B. P. Roques, S. F. J. Le Grice, and J. L. Darlix.** 1998. Involvement of HIV-1 nucleocapsid protein in the recruitment of reverse transcriptase into nucleoprotein complexes formed *in vitro.* J. Biol. Chem. **273:**33781–33786.
19. **Macura, S., and R. R. Ernst.** 1980. Elucidation of cross-relaxation in liquids by two-dimensional NMR spectroscopy. Mol. Phys. **41:**95–117.
20. **Mély, Y., H. de Rocquigny, N. Morellet, B. P. Roques, and D. Gérard.** 1996. Zinc binding to the HIV-1 nucleocapsid protein: a thermodynamic investigation by fluorescence spectroscopy. Biochemistry **35:**5175–5182.
21. **Morellet, N., N. Jullian, H. de Rocquigny, B. Maigret, J. L. Darlix, and B. P. Roques.** 1992. Determination of the structure of the nucleocapsid protein NCp7 from the human immunodeficiency virus type 1 by ^{1}H NMR. EMBO J. **11:**3059–3065.
22. **Morellet, N., H. De Rocquigny, Y. Mély, N. Jullian, H. Déméné, M. Ottmann, D. Gérard, J. L. Darlix, M. C. Fournié-Zaluski, and B. P. Roques.** 1994. Conformational behaviour of the active and inactive forms of the nucleocapsid NCp7 of HIV-1 studied by ^{1}H NMR. J. Mol. Biol. **235:**287–301.
23. **Morellet, N., H. Déméné, V. Teilleux, T. Huynh-Dinh, H. de Rocquigny, M.-C. Fournié-Zaluski, and B. P. Roques.** 1998. Structure of the complex between the HIV-1 nucleocapsid protein NCp7 and the single-stranded pentanucleotide d(ACGCC). J. Mol. Biol. **283:**419–434.
24. **Nilges, M., G. M. Clore, and A. M. Gronenborn.** 1988. Determination of three-dimensional structures of proteins from interproton distance data by dynamical simulated annealing from a random array of atoms. Circumventing problems associated with folding. FEBS Lett. **239:**129–136.
25. **Omichinski, J. G., G. M. Clore, K. Sakaguchi, E. Appella, and A. M. Gronenborn.** 1991. Structural characterization of a 39-residue synthetic peptide containing the two zinc binding domains from the HIV-1 p7 nucleocapsid protein by CD and NMR spectroscopy. FEBS Lett. **292:**25–30.
26. **Peliska, J. A., S. Balasubramanian, D. P. Giedroc, and S. J. Benkovic.** 1994. Recombinant HIV-1 nucleocapsid protein accelerates HIV-1 reverse transcriptase catalyzed DNA strand transfer reactions and modulates RNase H activity. Biochemistry **33:**13817–13823.
27. **Ramboarina, S., N. Morellet, M. C. Fournié-Zaluski, and B. P. Roques.** 1999. Structural investigation on the requirement of CCHH zinc finger type in nucleocapsid protein of human immunodeficiency virus 1. Biochemistry **38:**9600–9607.
28. **Ramboarina, S., N. Srividya, R. A. Atkinson, N. Morellet, B. P. Roques, J. F. Lefevre, Y. Mely, and B. Kieffer.** 2002. Effects of temperature on the dynamic behaviour of the HIV-1 nucleocapsid NCp7 and its DNA complex. J. Mol. Biol. **316:**611–627.
29. **Rein, A., L. E. Henderson, and J. G. Levin.** 1998. Nucleic-acid-chaperone activity of retroviral nucleocapsid proteins: significance for viral replication. Trends Biochem. Sci. **23:**297–301.
30. **Rémy, E., H. de Rocquigny, P. Petitjean, D. Muriaux, V. Theilleux, J. Paoletti, and B. P. Roques.** 1998. The annealing of $tRNA^{Lys,3}$ to human immunodeficiency virus type 1 primer binding site is critically dependent on the NCp7 zinc fingers structures. J. Biol. Chem. **27:**4819–4822.
31. **Summers, M. F., L. E. Henderson, M. R. Chance, J. W. Bess, T. L. South, P. R. Blake, I. Sagi, G. Perez-Alavarado, R. C. I. Sowder, D. R. Hare, and L. O. Arthur.** 1992. Nucleocapsid zinc fingers detected in retroviruses: EXAFS studies of intact viruses and the solution-state structure of the nucleocapsid protein from HIV-1. Protein Sci. **1:**563–574.
32. **Tanchou, V., D. Decimo, C. Péchoux, D. Lener, V. Rogemond, L. Berthoux, M. Ottmann, and J.-L. Darlix.** 1998. Role of the N-terminal zinc finger of human immunodeficiency virus type 1 nucleocapsid protein in virus structure and replication. J. Virol. **72:**4442–4447.
33. **Tsuchihashi, Z., and P. O. Brown** 1994. DNA strand exchange and selective DNA annealing promoted by the human immunodeficiency virus type 1 nucleocapsid protein. J. Virol. **68:**5863–5870.
34. **Williams, M. C., R. J. Gorelick, and K. Musier-Forsyth.** 2002. Specific zinc-finger architecture required for HIV-1 nucleocapsid protein's nucleic acid chaperone function. Proc. Natl. Acad. Sci. USA **89:**6472–6476.